Research article

Dynamic coordinated control strategy of a dual-motor hybrid electric vehicle based on clutch friction torque observer

Qicheng Xue, Xin Zhang *, Hongwei Chen, Meiling Yue, Teng Teng, Jiangbin Yu

Beijing Key Laboratory of Powertrain Technology for New Energy Vehicles, School of Mechanical, Electronic and Control Engineering, Beijing Jiaotong University, Beijing, 100044, China

ABSTRACT

The hybrid power system with dual motors and multiple clutches experiences significant torque fluctuation during mode switching process due to the different torque response characteristics of the motor and engine. To address this issue, this paper focuses on the estimation of clutch friction torque and the development of dynamic coordinated control strategies for the components. Firstly, based on the dynamic model of the novel dual-motor hybrid electric vehicle, a torque observer based on the Kalman filter algorithm is developed to predict the friction torque generated in the clutch sliding friction stage. Secondly, the control strategies are developed for the mode switching process from single-motor to dual-motor and from dual-motor to parallel drive on a co-simulation platform. Thirdly, a power level Hardware-In-the-Loop test platform is built, and the performance of the designed control strategies is verified by the HIL platform. The results show that for the mode switching process from dual-motor to parallel drive, compared with the control strategy using the engine target speed, the control strategy based on engine idle speed proposed in this paper reduces the clutch sliding friction work and the maximum longitudinal jerk of the vehicle by 42.5% and 25.4%, respectively.

1. Introduction

With the development and progress of society, the problems of environmental pollution and energy depletion are becoming more and more serious. New energy vehicles (NEVs) have drawn increasing attention in the automotive industry [1]. NEVs are mainly divided into pure electric vehicles (PEVs), fuel cell vehicles (FCVs), and hybrid electric vehicles (HEVs). The technical development of PEV is limited by the problems of high cost [2], short driving range [3], long charging time [4], battery electrolyte pollution [5], and so on. Fuel cells have technical issues of low fuel storage safety [6] and high cost, therefore FCVs are still under development and have relatively few applications. HEV, one of the most promising NEVs, has the advantages of long mileage and low-emission performance. However, due to the fact that HEV contains both engine and motor, it has a variety of operation modes, which makes its control strategy very complex. The research on HEV control strategy is of great significance in improving vehicle performance [7].

Control issues of HEV are usually defined by energy management control strategy (EMCS) [8,9] and dynamic coordinated control strategy (DCCS) [10]. There are three types of EMCS: rule-based logic threshold control strategy [11], intelligent control strategy [12, 13], and optimization algorithm-based control strategy [14,15]. HEVs drive in different working modes under different working conditions. Due to the significant difference between the dynamic responses of the engine and that of the motor, as well as the working state change of the clutch, an undesirable phenomenon of output torque fluctuation may be caused during the transient process of mode switching [10]. Therefore, it is necessary to design a DCCS for the mode switching process to improve the mode switching quality of the vehicle. Research on the core technology of HEVs has mainly focused on the steady-state EMCS, which is used for energy allocation and efficiency optimization. However, there is relatively limited research on the DCCS of torque output from different power sources during dynamic mode transitions. This paper selects the typical mode switching process of HEV to coordinate the torque between the motor, engine, and clutch.

The DCCSs proposed in the current literature for mode switching process can be classified into the following three categories. The first kind of DCCS adopts the strategy of "engine torque online estimation + motor torque compensation." In order to reduce the torque fluctuation of the output shaft, the lag of engine torque response can be compensated by the motor torque [16]. In order to obtain an accurate motor compensation amount, the actual output torque of the engine is measured or estimated. Ref. [17] collected the transient speed and throttle opening signals of the engine's actual working process and obtained the engine's estimated torque by querying the steady-state map of the engine. Refs. [18,19] built the engine average value model and proposed a DCCS to compensate for the engine torque in different switching stages. The second kind of DCCS adopts different control algorithms to dynamically compensate for the torque of the gearbox system directly to ensure the continuity and stability of vehicle power transmission. Ref. [20] proposed a forward feedback control strategy based on the reference model to reduce the fluctuation of system output power during the clutch engagement process. Ref. [21] took the clutch torque as the optimization variable and proposed a torque coordinated control strategy based on data-driven predictive control, effectively reducing the vehicle jerk and shortening the mode switching time. Ref. [22] proposed a DCCS of "engine torque estimation + jerk prediction model," which significantly improved the driving performance of the vehicle. The third kind of DCCS is to divide the mode switching process into several sub-stages, and design the corresponding controller for each sub-stage. In Ref. [23], the mode switching process of parallel HEV was divided into four stages, and the disturbance observer was used in the second to fourth stages, effectively suppressing the output torque fluctuation. Ref. [24] divided the mode switching process of HEV into five stages, and a hierarchical control structure was proposed. The upper controller adopted H∞ robust control, and the lower controller adopted L2 gain robust tracking control, which effectively shortened the switching time. Ref. [25] divided the mode switching process of parallel HEV into three stages, and designed a fuzzy-PI controller and an adaptive sliding mode controller to coordinate the speed and the torque of the engine and the motor to ensure the stability of power transmission. In addition, Refs. [26,27] also studied the mode switching process of HEVs equipped with planetary system coupling mechanisms. The structural characteristics of the planetary system enabled mutual communication between the three power sources: the engine, the generator and the driving motor. In this way, the torque of the engine can be obtained in real time so that coordinated control during the mode switching process can be achieved. It is worth noting that the coordinated control strategies of electric vehicles are also used for ancillary services and vehicle-to-grid systems. Refs. [28,29] studied control technologies based on battery health status in vehicle-to- grid technology, while ref. [30] reviewed the latest applications and frameworks of communication technology in distributed generation. At present, the coordinated control technology between vehicle-to-grid technology, communication technology, and new energy vehicles is also a new research hotspot.

It can be summarized from the above research that most researchers focus on the torque DCCS of engine and motor, i.e., using the fast response characteristics of the motor to compensate for the engine torque in real time. However, the influence of clutch state change on the switching quality during the mode switching process is rarely considered. The clutch is a key component for achieving excellent performance during the mode switching process of HEVs. The optimal control method in Ref. [31] and the model predictive control method in Ref. [32] solve the problem of optimal trajectory tracking. In addition, some nonlinear control methods, such as fuzzy sliding control [33] and nonlinear feedforward feedback control [34], have achieved precise clutch control effects. The above literature only focuses on the study of clutch engagement control. For hybrid power system (HPS) with clutches, in Ref. [35], a robust tracking controller is designed to perform the accurate position tracking control. Ref. [36] proposed an adaptive feedforward control method for clutch torque based on the clutch friction model. In Ref. [37], Model predictive feed-forward control and robust H∞ feedback control were designed to guarantee the dynamic performance in the clutch slipping phase of the mode transition. Ref. [38] presented an optimal controller based on off-line computation of control gain profiles for clutch engagement during gear shifts. Much of the research on the multi-plate wet clutch has focused on filling control [39], slip control [40], and adaptive control [41] to obtain a smooth clutch-to-clutch shift [42] or launching process [43]. Traditional clutch engagement control methods cannot be directly used in hybrid power systems' mode conversion. In addition, the clutch engagement control performance should also consider the dynamic characteristics of the clutch torque. Based on the changes in the torque transmitted by the clutch or its friction torque, consider the torque DCCS of the clutch, engine, and motor.

Based on the above literature, compared to the powertrain system of conventional vehicles, the powertrain system of HEVs is relatively more complex and the working modes are more diverse, which puts higher requirements on the quality of their dynamic control. In order to further improve the smoothness, comfort, and reliability of the mode switching process of HEVs, reduce clutch sliding friction work, and shorten the time of power interruption, this paper takes dual-motor HEV as the research object, mainly studying the DCCS of the mode switching process.

For HEVs, the core task of the working mode switching process is to change the operating state of the actuator, which involves controlling the engagement and disengagement states of the clutch or synchronizer. In this paper, the key control issues related to changes in the working status of the actuator include the following aspects: (1) The dual-motor HPS studied in this paper involves

multiple power sources and actuators. Therefore, in the study of mode switching process, the DCCS of multiple components will be involved. For example, this paper proposes a DCCS for clutch friction torque and motor torque, as well as a DCCS for motor speed control and clutch engagement control. (2) The change in the working state of the clutch is a continuous process, and there is still a sliding friction stage between the separation stage and the locking stage. The friction torque generated by the sliding process is time-varying and can't be measured using sensors. This paper uses the Kalman filter algorithm (KFA) to estimate the friction torque generated by the clutch. (3) In order to make the actuator change its working state more smoothly (for example, the clutch changes from a disengaged state to an engaged state), the motor speed can be actively adjusted to make the speed of both ends of the actuator close. For the control algorithm of motor speed, the paper will adopt a composite control algorithm based on fuzzy-PID-bangbang. (4) The change in the working state of the actuator is a sign of the completion of the mode switching process, so effective control of the actuator is also one of the key control issues in HPSs.

In conclusion, mode switching is a transient process, and the system structure and control strategy are crucial to its control effectiveness. A HPS with development value and promotion potential is an effective and desirable solution. Motivated by this issue, this paper proposes a new HPS with dual motors and three clutches.

The main contribution is given as follows. Firstly, an observer model for the friction torque during the clutch engagement process was established using the KFA, solving the problem of the inability to measure the friction torque directly. Secondly, a multi-stage DCCS for the mode switching process was proposed, achieving coordinated control of clutch, motor, and engine. Thirdly, the control strategy proposed in this paper was validated based on simulation platforms and Hardware- In-the-Loop (HIL) platforms. In addition, the study of the mode switching process in this paper has important reference significance for the coordinated control research of other transition processes in HPSs, such as gear shifting and vehicle startup processes.

The rest of this paper is organized as follows. The studied novel HEV and the related model construction are described in Section II and III, respectively. Section IV presents the DCCS. In Section V, the simulation of the proposed DCCS is performed and the results are analyzed and discussed. The experimental evaluation of the proposed DCCS is conducted in Section VI via comparison studies. The main conclusions are drawn in Section VII.

2. HPS configuration and working principle

2.1. Configuration and parameters

Since the launch of the first generation Prius equipped with a dual-motor HPS by Toyota Motor Company in Japan in 1997, its novel configuration, superior power performance, and good fuel economy have attracted the attention of the automotive industry worldwide, and have also sparked a wave of development of dual-motor HEVs in the automotive industry. Afterwards, dual-motor HPSs such as the General Volt and Honda i-MMD were introduced one after another. Diversifying hybrid technology routes is a development trend in the automotive industry. Different hybrid technology routes have their advantages and disadvantages, and there is no best technology route or product. Each enterprise needs to develop the most suitable technology route and configuration for its advantages and strategic planning. Developing HEVs has become a top priority for automotive companies around the world, and developing advanced electromechanical coupling systems plays a crucial role in improving the competitiveness of HEVs.

This paper proposes a HPS scheme that includes dual motors. The system can output torque through three gears, expanding the range of power source output torque and allowing the engine and motor to work more efficiently, thereby improving the vehicle's power and fuel economy. During the mode switching process, torque coordination control of the power source and clutch can ensure that the vehicle always has driving force during the transient switching process, thereby eliminating power interruption and improving the smoothness and comfort of the mode switching process.

The powertrain system studied in this paper is a novel dual-motor HPS. The system configuration is shown in Fig. 1, and its main parameters are listed in Table 1. In the HPS, the power transmission system is composed of an internal combustion engine (ICE),
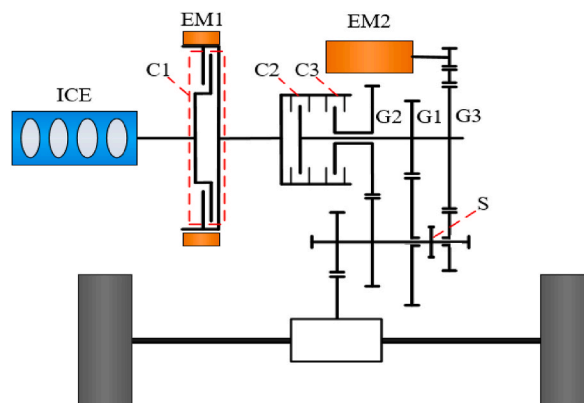
Fig. 1. Schematic diagram of the configuration of the HPS.

electric motor 1 (EM1), electric motor 2 (EM2), and a three-speed gearbox. The executive system of mode switching comprises three wet multi-plate clutches (C1, C2, and C3), a synchronizer (S), and its hydraulic mechanism. Among them, the working state of C1 enables the connection and separation between ICE and EM1, the working state of C2 and C3 enables the connection and separation between EM1 and the three-speed gearbox, and the engagement and disengagement of C2, C3, and S enables the switching between the three gears of the system.

2.2. Analysis of working mode

The HPS is subject to different working modes depending on the demanded power when the vehicle is running. For example, when the vehicle is in a state of low power demand, the driving torque of the vehicle is usually provided by the EM2 alone in pure electric mode; When the vehicle is in a medium power demand state, the EM1 and the EM2 jointly provide the driving torque for the vehicle in pure electric mode; When the vehicle is in a state of high power demand, the vehicle works in a hybrid drive mode, i.e., the engine and dual motors drive the vehicle together. The vehicle can be switched between different working modes by changing the working state of the engine, the motor, and the clutch.

Taking the gearbox working in G1 as an example (C3 is in the disengaged state), the working states (disengaged or engaged) of C1 and C2 are arranged and combined, and further combined with the working states of EM1, EM2 (in the power generation mode or electric drive mode), and ICE (whether it is running), the HPS proposed in this paper can have five typical working modes, as shown in Table 2. The power transmission route diagram under different working modes is shown in Fig. 2.

3. Powertrain modeling

3.1. Engine model

The Engine is a highly complex nonlinear system, and its real model is difficult to establish accurately. Engine modeling methods are generally divided into theoretical and experimental [44,45]. Theoretical modeling requires detailed thermodynamic, combustion, and dynamic analysis of the engine's working process, which is complex and time-consuming. Compared with the theoretical modeling method, the experimental modeling method is relatively simple, and the engine's characteristic data required in the model can be easily obtained through bench tests. Because when conducting simulation analysis on HPSs, it is optional to know the actual working conditions inside the engine. Only the input and output data of the engine need to be obtained. Therefore, this paper uses experimental modeling methods in the simulation modeling of HPSs. The engine torque dynamic response is influenced by many factors, making it difficult to establish an accurate model.

The primary resistance during the engine start-up process is the compression resistance of the cylinder, the frictional resistance of the piston ring, the frictional resistance of the piston skirt, the frictional resistance of the valve mechanism, the inertial force of the reciprocating motion of the piston assembly, and the operating resistance of the accessory components. The starting resistance torque of the engine is complex and closely related to temperature, lubrication status, etc. For the study of HPS mode switching control strategy (MSCS), it is only necessary to know the input and output characteristics of the engine starting process, without needing to understand the actual working process of the engine internally. The starting drag torque and torque output characteristics of the engine studied in this paper are shown in Figs. 3 and 4, respectively.

The start-up engine is one of the key control processes in the mode switching of HEVs. This control process requires not only the

Table 1
Main Parameters of the novel HEV.

Item	Parameter/Unit	Value
Vehicle	Vehicle mass/kg	1545
	Wheel radius/m	0.347
	Drag coefficient	0.36
	Windward area/m^2	2.638
	Rolling resistance coefficient	0.008
EM1	Type	PMSM
	Peak torque/Nm	160
	Peak power/kW	55
	Peak speed/(r/min)	6200
EM2	Type	PMSM
	Peak torque/Nm	155
	Peak power/kW	70
	Peak speed/(r/min)	12,000
ICE	Peak torque/Nm	210
	Peak power/kW	110
	Maximum speed/(r/min)	5500
Gearbox	First gear speed ratio	2.03
	Second gear speed ratio	1.01
	Third gear speed ratio	0.63
Main reducer	Gear ratio	3.7

Table 2

The working state of power sources and clutch in each working mode.

Working mode	ICE	EM1	EM2	C1	C2
Single-motor pure electric mode (Mode SP)	Stopped	Stopped	Electric drive	Disengaged	Disengaged
Dual-motor pure electric mode (Mode DP)	Stopped	Electric drive	Electric drive	Disengaged	Engaged
Series drive mode (Mode SD)	Running	Power generation	Electric drive	Engaged	Disengaged
Parallel drive mode (Mode PD)	Running	Electric drive	Electric drive	Engaged	Engaged
Engine drive mode (Mode ED)	Running	Stopped	Stopped	Engaged	Engaged

establishment of a steady-state torque model for the engine, but also the establishment of a dynamic torque model. Due to the fact that this paper doesn't consider the issue of engine emissions, the engine's dynamic characteristics are characterized by a combination of the steady-state look-up table model and the first-order inertia delay link [46].

The engine output torque is

$$T_E = \frac{1}{\tau_e s + 1} f(\omega_E, \alpha) \tag{1}$$

where T_E and ω_E are the output torque and speed of the engine, respectively, τ_e is the time constant of engine torque response, α is the throttle opening, s is the Laplace operator, $f(\omega_E, \alpha)$ is the mapping function among engine steady torque, throttle opening, and engine speed, which is obtained from engine bench test data.

3.2. Motor model

Permanent magnet synchronous motor (PMSM) is widely used in automobile power systems because of its simple structure, high power density, and high efficiency. Similar to the engine, the dynamic models of EM1 and EM2 also adopt the method of combining experimental modeling and theoretical modeling.

While the motor responds to the target torque, it consumes or generates electricity, and the corresponding current is a function of output torque, motor speed, battery voltage, and motor efficiency.

When the motor is in electric drive mode, the demand current of the motor is

$$I_{m\_d} = \frac{T_m \omega_m}{9549 V_m \eta_m} \tag{3}$$

When the motor is in power generation mode, the output current of the motor is

$$I_{m\_g} = \frac{T_m \omega_m \eta_m}{9549 V_m} \tag{4}$$

where I_{m_d} and I_{m_g} denote the battery's discharge and charging current, respectively. V_m denotes the terminal voltage of the battery. η_m denotes the motor efficiency, which is a function of the motor rotor speed and the actual output torque of the motor [47].

For dynamic coordination control during mode switching process, it is necessary to coordinate the torque of the power source and other relevant components. The main purpose is to compensate for torque fluctuations to the greatest extent possible by utilizing the rapid torque response of the motor. Therefore, the rapid torque response of the motor is a prerequisite for performing dynamic co-ordination control.

The external characteristic curves of the two motors used in this paper are shown in Fig. 5. By processing the data of the motor operating characteristics obtained by the experiment, and the power loss characteristic diagram of the two motors can be obtained, as shown in Fig. 6. The trend of power loss change for EM1 and EM2 is similar; that is, the larger the motor's speed and torque, the greater the power loss. EM1's peak torque is 160 Nm, and its maximum speed is 6200 r/min; EM2's peak torque is 155 Nm, and its maximum speed is 12,000 r/min. As an auxiliary motor, EM1 has a smaller working speed range and a lower maximum speed, mainly used to start the engine. EM2 is mainly used to drive the vehicle.

The torque response time of the motor is much less than that of the engine, and the main research content of this paper is the control of motor torque during the mode switching process. Hence, the established motor model only needs to simulate the real torque response characteristics of the motor accurately. Therefore, there is no need to consider the three-phase current, three-phase voltage, and magnetic loss when modeling the motor. Thereby the motor model can be simplified. Generally, the first-order response of the motor demand torque can be used to reflect the response characteristics of the motor to the target torque, and the output torque T_m of the motor can be expressed as:

$$T_m = \begin{cases} min(T_{m\_tar}, T_{m\_max}) \cdot \dfrac{1}{\tau_m s + 1} & if \ T_{m\_tar} > 0 \\ max(T_{m\_tar}, T_{m\_min}) \cdot \dfrac{1}{\tau_m s + 1} & if \ T_{m\_tar} < 0 \end{cases} \tag{2}$$

where τ_m denotes the time constant of motor torque response, T_{m_tar} denotes the target torque of the motor. T_{m_max} denotes the
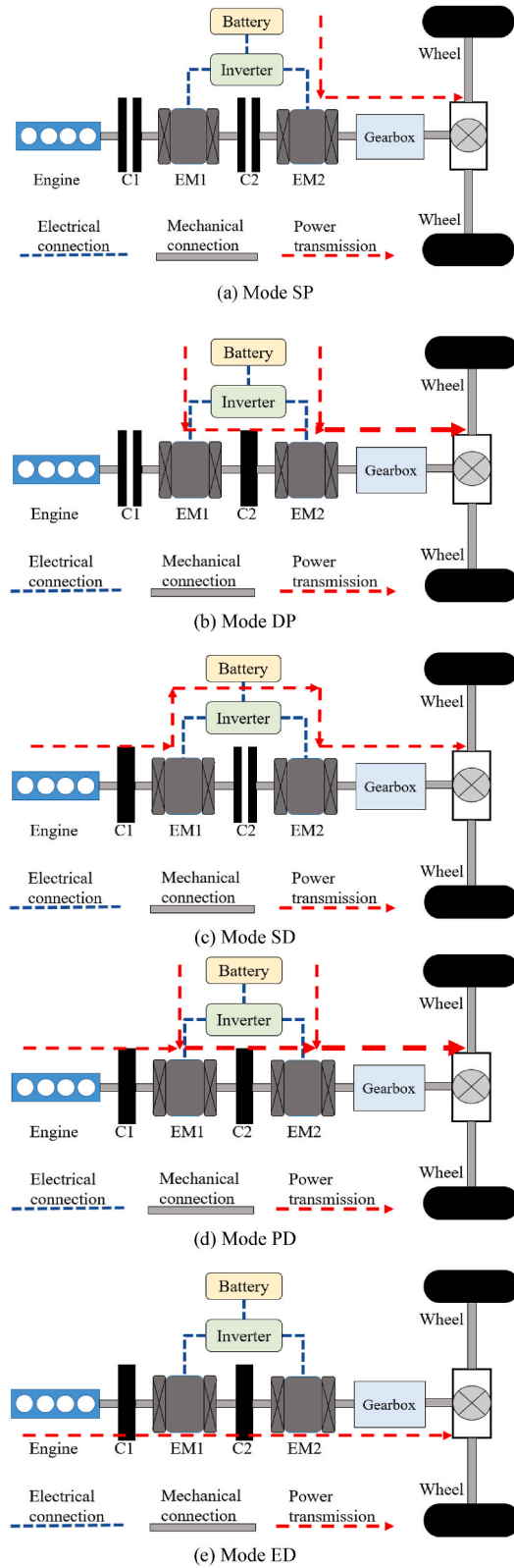
Fig. 2. Schematic diagram of power transmission route of each working mode.
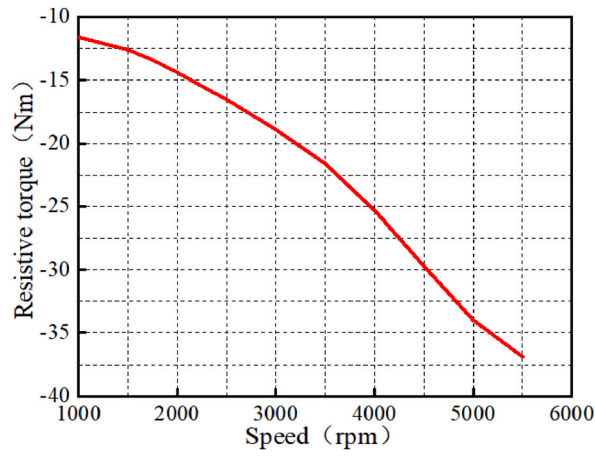
Fig. 3. Engine starting drag torque map.
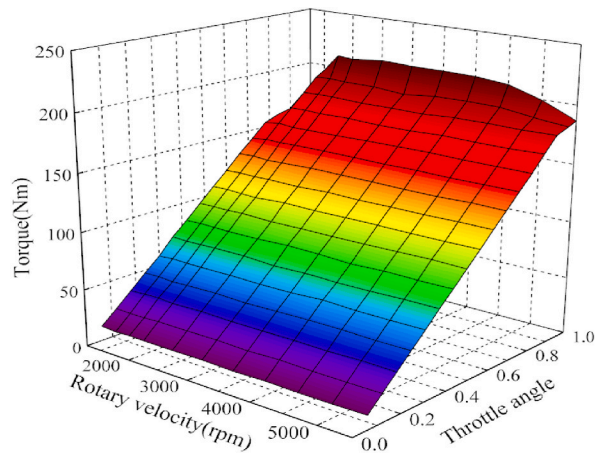
Fig. 4. Engine output torque map.
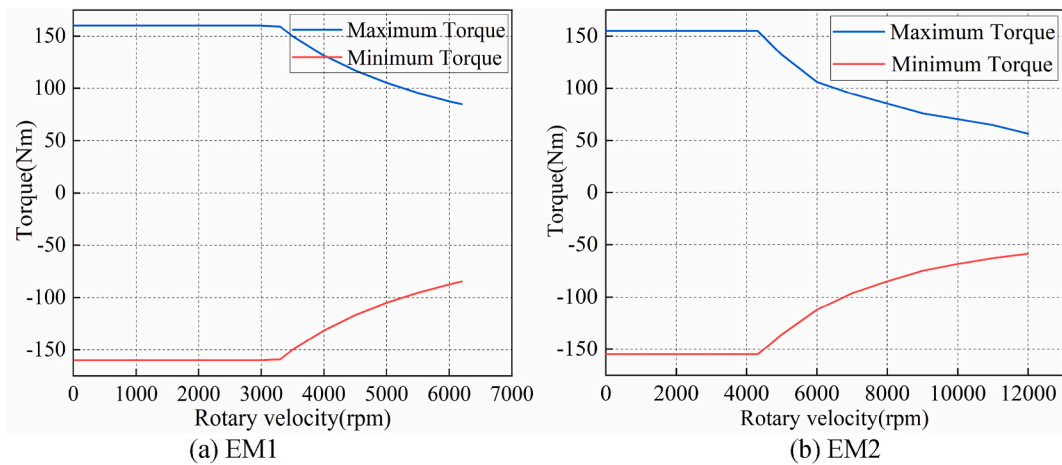
Fig. 5. External characteristic curves of motors.
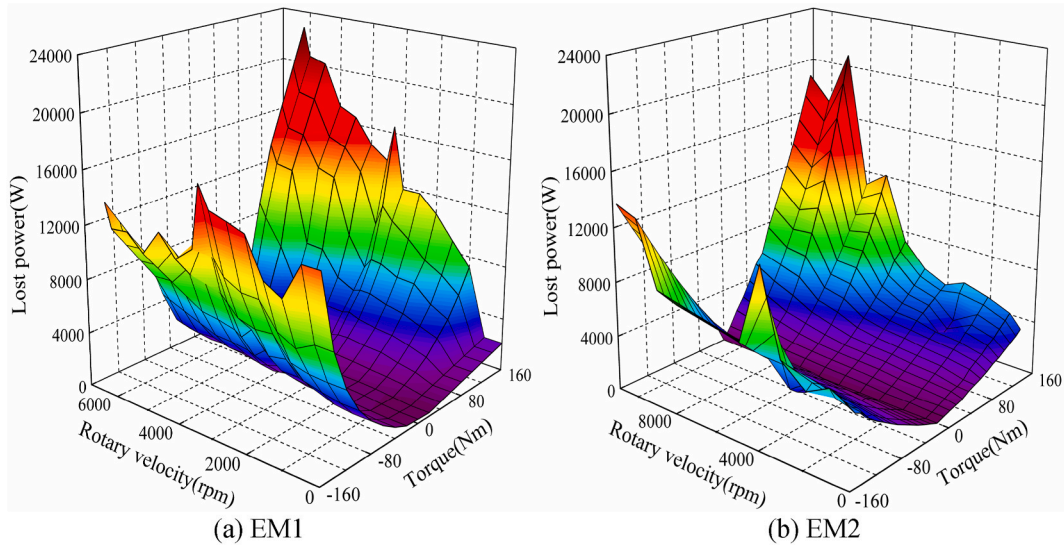
Fig. 6. Map of motor power loss.

maximum output torque of the motor. T_{m_min} denotes the maximum generating torque of the motor.

3.3. Wet multi-plate clutch model

The wet multi-plate clutch is an essential part of the power coupling system of the HEV, and its engagement and disengagement directly affect the change in the running state of the vehicle. The working principle of a wet multi-plate clutch is shown in Fig. 7. When the clutch is about to be engaged, the clutch hydraulic control system will increase the oil pressure of the clutch hydraulic cylinder by controlling the proportional solenoid valve (PSV). When the pressure force generated by the oil pressure pushing the piston can overcome the resistance of the spring, the driving plate and driven plate of the clutch begin to engage. The engagement of the wet multi-plate clutch is completed after a period of time, and its process can be divided into three stages, as shown in Fig. 8.

The first stage ($0 \sim t_0$): the complete separation stage, also known as the empty stroke stage. At this stage, there is no friction resistance between the driving and driven plates of the clutch. Under the hydraulic control system, the piston pushes the driving plate of the clutch to move towards the driven plate to gradually eliminate the gap between the driving and driven plates of the clutch. At this stage, the contact pressure of the driving and driven plates of the clutch is almost zero, and no torque is transmitted.

The second stage ($t_0 \sim t_1$): the sliding friction stage. At this stage, the driving and driven plates of the clutch are contacted. With increased clutch engagement pressure, the torque transmitted by the clutch increases gradually, and the speed difference between the driving and driven plates of the clutch ($\Delta\omega$) gradually decreases.

The third stage ($t_1 \sim$): the locking stage. After entering this stage, the speed difference between the driving plate and the driven plate of the clutch is zero. At this stage, it is used as a torque transmission device, and the torque transmitted by the clutch is a particular value.

The main parameters of the wet multi-plate clutch are listed in Table 3.

The clutch hydraulic control system comprises a clutch actuator and a PSV. The separation and engagement of the wet multi-plate clutch can be realized during the mode switching process through the control of the clutch engagement pressure. The technical parameters of the direct-drive PSV used in this paper are listed in Table 4.
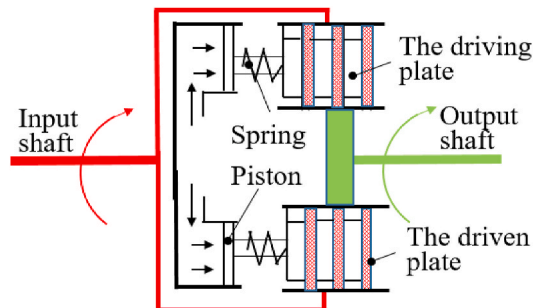
Fig. 7. Working principle diagram of wet multi-plate clutch.
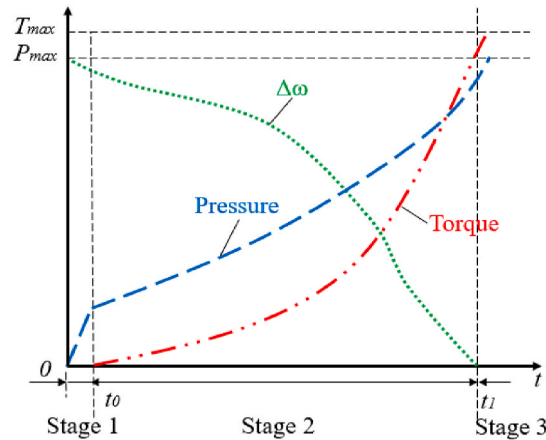
Fig. 8. Schematic diagram of engagement process of wet multi-plate clutch.

The current-pressure performance curve of the PSV is shown in Fig. 9.

From the technical parameters of the PSV, it can be seen that the response speed of the clutch control system is very fast, which is much greater than the torque response speed of the engine, and there is little difference with the torque response speed of the motor. From the current-pressure performance curve of the PSV, it can be seen that the output oil pressure of the control system is approximately linear with the control current, indicating good control performance. Therefore, in clutch engagement, the clutch oil pressure can be dynamically controlled to reduce the fluctuation of torque transmission.

3.4. Model validation

In this paper, the engine model, motor model, power battery model, clutch model, hydraulic cylinder model, vehicle dynamics model and driver model are established in AMESim software. Both the completed vehicle and powertrain system model are shown in Fig. 10.

Based on the New European Driving Cycle (NEDC), the vehicle model based on AMESim software is simulated and verified, and the result is shown in Fig. 11. It can be seen from the Fig. 11 that the simulation speed can well follow the target speed under NEDC working condition, which lays a foundation for the follow-up research on the MSCS of HEV.

4. Dynamic coordinated control strategy development

The analysis in Section 2.2 shows that the novel HEV studied in this paper mainly has five driving modes, and theoretically, mode switching can be realized between any two modes. As the engine start-stops are involved in the mode switching process, this paper divides the mode switching into two types: mode switching without engine start-stops and mode switching with engine start-stops. Among them, for the mode switching without engine start-stops, this paper selects the mode switching process from single-motor pure electric drive (Mode SP) to dual-motor pure electric drive (Mode DP) as a representative working condition. This paper selects the mode switching process from dual-motor pure electric drive (Mode DP) to parallel drive (Mode PD) as a typical working condition for the mode switching with engine start-stops.

4.1. Overall control flow design of the mode switching process

4.1.1. Switch from mode SP to mode DP

For the mode switching process from Mode SP to Mode DP, the control flow chart of mode switching designed in this paper is shown in Fig. 12. Based on the operating status of each component, the process is divided into four stages: single-motor drive stage, motor speed regulation stage, clutch engagement stage, and dual-motor drive stage. (1) Single-motor drive stage: During the single-motor drive stage of the HPS, the synchronizer is fully engaged, and clutches C2 and C3 are completely disengaged. EM2 is the sole power source, and power is transmitted through gear pair G1 in the transmission mechanism. (2) Motor speed regulation stage: When

Table 3
Main parameters of wet multi-plate clutch.

Clutch	Number of friction surfaces	Outer diameter of friction surface/mm	Inner diameter of friction surface/mm	Coefficient of friction
C1	8	129	108.1	0.12
C2	10	120.1	107	0.12
C3	12	126.7	110.8	0.12

Table 4
Technology parameters of PSV.

Item	Working oil pressure	Supply voltage	Current range	Response time
Parameter value	20 bar	12 ± 3 V	0~1.5 A	<30 ms
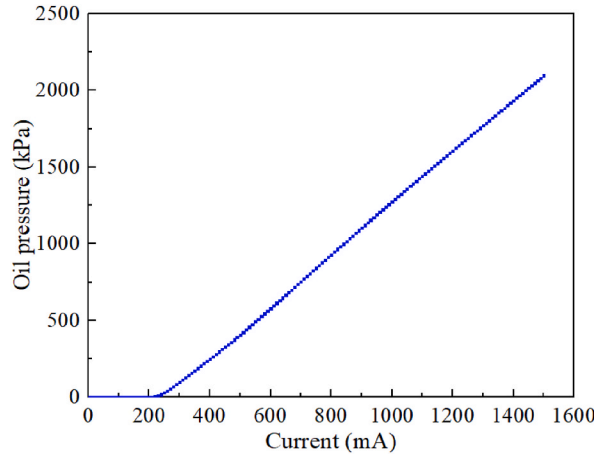
Fig. 9. Current-pressure performance curve of PSV.
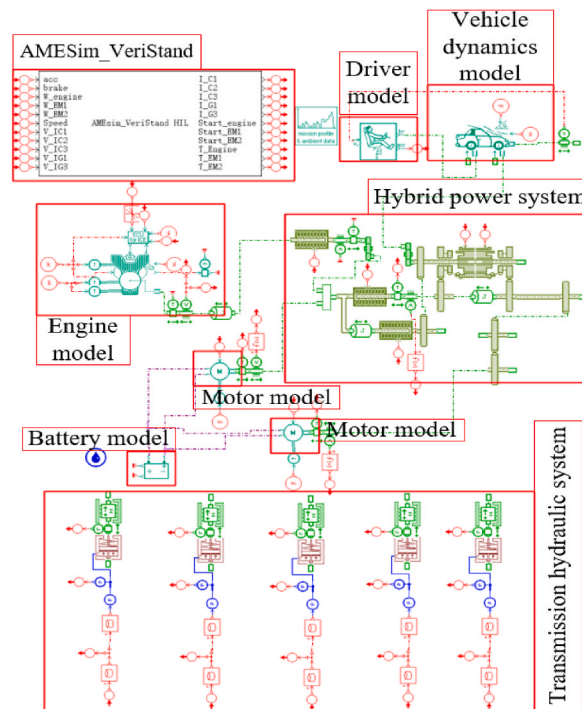
Fig. 10. Model diagram of the novel HEV.

the HPS operates in the EM1 speed regulation stage, the working status of the synchronizer, C2, and C3 remains consistent with the first stage. EM2 is the only power source, and EM1 starts and operates in speed control mode. The speed control algorithm for EM 1 is fuzzy-PID-bangbang. (3) Clutch engagement stage: After the completion of EM1 speed regulation, the HPS enters the slipping friction stage of C2. (4) Dual-motor drive stage: Once the C2 is fully engaged, the HPS enters the dual-motor drive stage. During this stage, both the synchronizer and clutch C2 are fully engaged, and both EM1 and EM2 act as power sources, with power transmitted through gear pair G1 in the transmission mechanism.
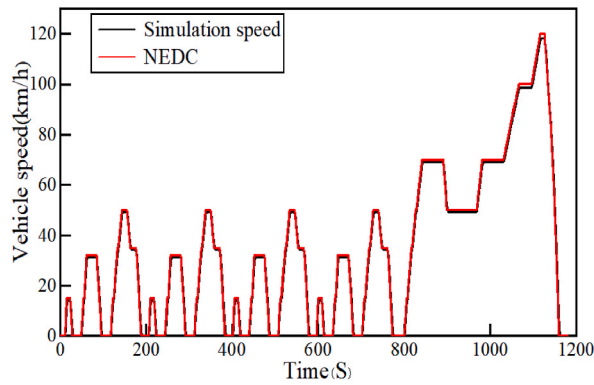
Fig. 11. Simulation results based on NEDC working conditions.
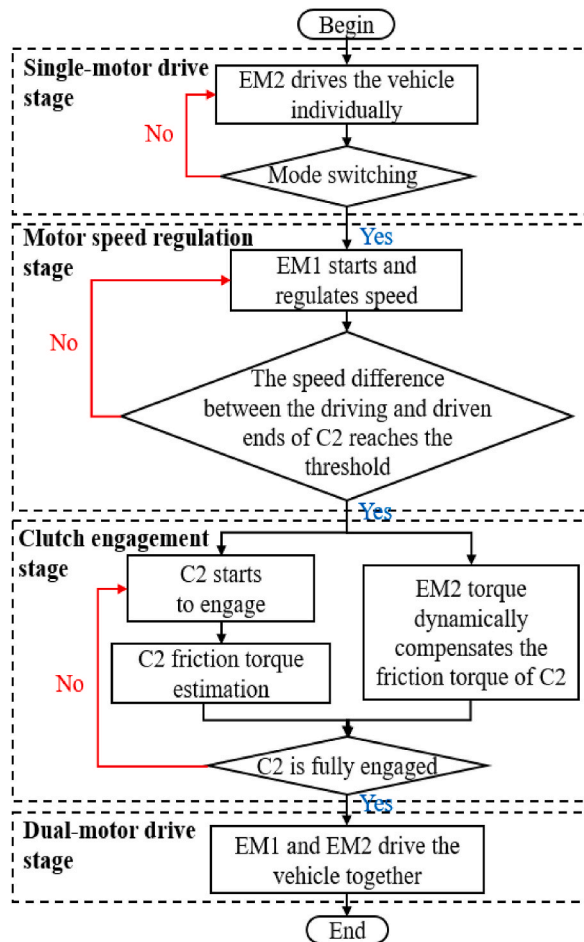
Fig. 12. Control flow chart of switching from Mode SP to Mode DP.

In summary, for the mode switching process from Mode SP to Mode DP, this study developed a sequential DCCS of single-motor drive – motor speed control – clutch engagement control – dual-motor drive. Specifically, in the C2 slipping friction stage, a torque DCCS with clutch friction torque estimation and motor torque dynamic compensation has been further developed.

4.1.2. Switch from mode DP to mode PD

The switching process from Mode DP to Mode PD is divided into four stages: dual-motor drive, engine start, engine speed regulation, and parallel drive. The control flow chart is shown in Fig. 13.

4.2. Design of clutch friction torque observer

Since the friction torque generated in the sliding friction stage of the engagement process of wet multi-plate clutch is difficult to measure directly, the friction torque is estimated by KFA based on the vehicle longitudinal dynamics model, and the measurable state information of vehicle powertrain systems such as motor speed and gearbox input (output) shaft speed. Taking the switching process from Mode SP to Mode DP as an example, the observer of the friction torque of C2 is designed.

4.2.1. Dynamic analysis of mode switching process

In this paper, the following assumptions are made when modeling the dynamics of the novel HEV.

a In the modeling process, only the vehicle running on a straight line is considered, and special working conditions such as turning are not considered.
b In this paper, each part of the automobile is simplified and modeled by the centralized mass method.
c The torsional vibration, damping, and friction resistance in the transmission system are ignored.
d The influence caused by the slip and slip movement between the wheel and the ground is ignored.

The schematic diagram of the dynamic model is shown in Fig. 14.
The dynamic analysis of the four stages of the mode switching process from Mode SP to Mode DP is as follows.

① Single-motor drive stage

At this stage, the system contains three degrees of freedom. The torque of EM2 is transmitted to the gearbox output shaft through the first gear (G1). There is a definite kinematic relationship between the speed of EM2, the speed of the gearbox input shaft and the output shaft.
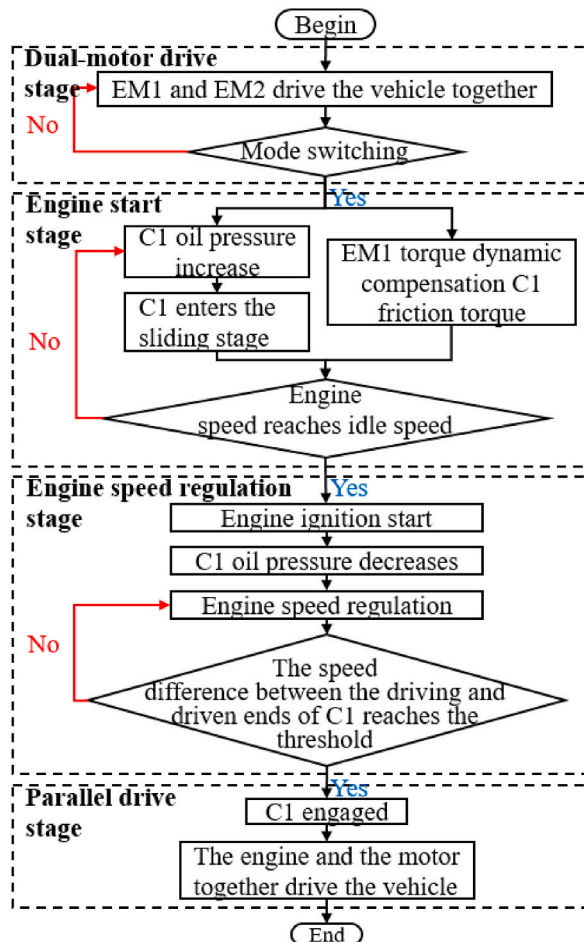
Fig. 13. Control flow chart of switching from Mode DP to Mode PD.

$$\frac{\omega_{EM2}}{i_{g0}} = \omega_{in} = \omega_{out} \bullet i_{G1} \tag{5}$$

The power of EM2, the vehicle's resistance, and the moment of inertia of each gearbox component are equivalent to the gearbox's output shaft. The dynamic equation of this stage can be obtained as follows:

$$T_{EM2} \bullet i_{g0} \bullet i_{G1} - T_{out} = J_{EM2} \bullet \frac{d_{\omega_{EM2}}}{d_t} \bullet i_{g0} \bullet i_{G1} + J_{in} \bullet \frac{d_{\omega_{in}}}{d_t} \bullet i_{G1} + J_{out} \bullet \frac{d_{\omega_{out}}}{d_t} \tag{6}$$

From equations (5) and (6), it can be obtained that:

$$T_{EM2} \bullet i_{g0} \bullet i_{G1} - T_{out} = \left[\left(J_{EM2} \bullet i_{g0}{}^2 + J_{in} \right) \bullet i_{G1}{}^2 + J_{out} \right] \bullet \frac{d_{\omega_{out}}}{d_t} \tag{7}$$

For the EM1:

$$J_{EM1} \bullet \frac{d_{\omega_{EM1}}}{d_t} = 0 \tag{8}$$

For the engine:

$$J_e \bullet \frac{d_{\omega_e}}{d_t} = 0 \tag{9}$$

② Motor speed regulation stage

At this stage, the system contains three degrees of freedom. Since the C2 is in the disengaged state, there is a speed difference between the driving and driven plates of C2, that is, $\omega_{EM1} \neq \omega_{in}$.

The dynamic equation of this stage is:

$$T_{EM2} \bullet i_{g0} \bullet i_{G1} - T_{out} = \left[\left(J_{EM2} \bullet i_{g0}{}^2 + J_{in} \right) \bullet i_{G1}{}^2 + J_{out} \right] \bullet \frac{d_{\omega_{out}}}{d_t} \tag{10}$$

For the EM1:

$$J_{EM1} \bullet \frac{d_{\omega_{EM1}}}{d_t} = T_{EM1} \tag{11}$$

For the engine:

$$J_e \bullet \frac{d_{\omega_e}}{d_t} = 0 \tag{12}$$

③ Clutch engagement stage

At this stage, the C2 enters the sliding state and transmits friction torque. The dynamic equation currently is:
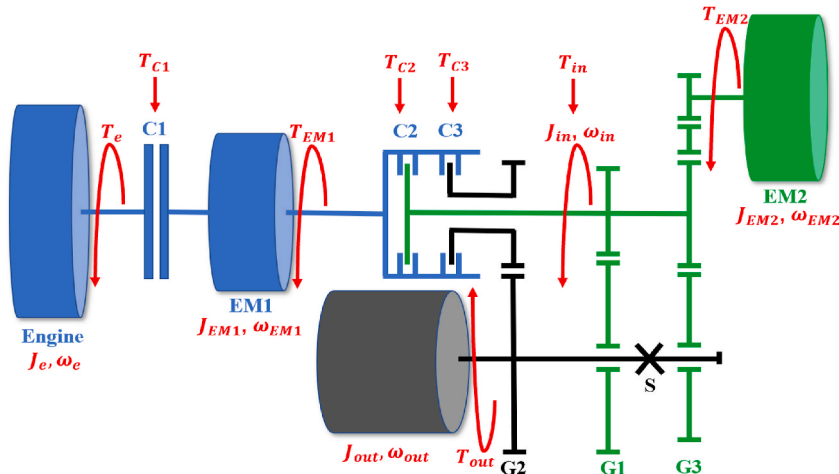
Fig. 14. Schematic diagram of dynamic model.

$$\text{T}_{EM2} \bullet i_{g0} \bullet i_{G1} + \text{T}_{C2} \bullet i_{G1} - \text{T}_{out} = \left[\left(\text{J}_{EM2} \bullet i_{g0}{}^2 + \text{J}_{in} \right) \bullet i_{G1}{}^2 + \text{J}_{out} \right] \bullet \frac{d_{\omega_{out}}}{d_t} \tag{13}$$

For the EM1:

$$\text{J}_{EM1} \bullet \frac{d_{\omega_{EM1}}}{d_t} = \text{T}_{EM1} - \text{T}_{C2} \tag{14}$$

For the engine:

$$\text{J}_e \bullet \frac{d_{\omega_e}}{d_t} = 0 \tag{15}$$

④ Dual-motor drive stage

After C2 is fully engaged, the system contains 2 degrees of freedom. There is a definite kinematic relationship among the four variables of EM1 speed, EM2 speed, gearbox input shaft and output shaft speed.

$$\omega_{EM1} = \frac{\omega_{EM2}}{i_{g0}} = \omega_{in} = \omega_{out} \bullet i_{G1} \tag{16}$$

The dynamic equation of this stage is:

$$\text{T}_{EM1} \bullet i_{G1} + \text{T}_{EM2} \bullet i_{g0} \bullet i_{G1} - \text{T}_{out} = \text{J}_{EM1} \bullet \frac{d_{\omega_{EM1}}}{d_t} \bullet i_{G1} + \text{J}_{EM2} \bullet \frac{d_{\omega_{EM2}}}{d_t} \bullet i_{g0} \bullet i_{G1} + \text{J}_{in} \bullet \frac{d_{\omega_{in}}}{d_t} \bullet i_{G1} + \text{J}_{out} \bullet \frac{d_{\omega_{out}}}{d_t} \tag{17}$$

From equations (16) and (17):

$$\text{T}_{EM1} \bullet i_{G1} + \text{T}_{EM2} \bullet i_{g0} \bullet i_{G1} - \text{T}_{out} = \left[\left(\text{J}_{EM1} + \text{J}_{EM2} \bullet i_{g0}{}^2 + \text{J}_{in} \right) \bullet i_{G1}{}^2 + \text{J}_{out} \right] \bullet \frac{d_{\omega_{out}}}{d_t} \tag{18}$$

For the engine:

$$\text{J}_e \bullet \frac{d_{\omega_e}}{d_t} = 0 \tag{19}$$

where T_e, T_{EM1}, and T_{EM2} represent the output torques of the engine, EM1 and EM2 respectively. T_{C1}, T_{C2}, T_{C3}, and T_S represent the torque transmitted by C1, C2, C3, and synchronizer respectively. T_{in} and T_{out} represent the torque of the gearbox input shaft and the equivalent resistance torque on the gearbox output shaft, respectively. J_e, J_{EM1}, J_{EM2}, J_{in}, and J_{out} represent the equivalent moment of inertia on the engine, EM1, EM2, gearbox input shaft and output shaft, respectively. ω_e, ω_{EM1}, and ω_{EM2} are the rotational speeds of the engine, EM1, and EM2, respectively. ω_{in} and ω_{out} are the rotational speeds on the gearbox input and output shafts, respectively. i_{g0} is the speed ratio of the reducer fixedly connected with the output end of EM2. i_{G1}, i_{G2}, and i_{G3} are the speed ratios of the gearbox's first, second, and third gears, respectively.

4.2.2. Design of the observer model of clutch friction torque based on KFA

In the process of clutch sliding engagement, the dynamic differential equation of EM2 and C2 is equation (13).
Definition:

$$\text{T}_{EM2} \bullet i_{g0} - \frac{\text{T}_{out}}{i_{G1}} = \text{T}_{mf} \tag{20}$$

$$\left[\left(\text{J}_{EM2} \bullet i_{g0}{}^2 + \text{J}_{in} \right) \bullet i_{G1}{}^2 + \text{J}_{out} \right] \bullet \frac{1}{i_{G1}{}^2} = \text{J}_c \tag{21}$$

The simplified dynamic equation of the transmission system can be written as:

$$T_{mf} - T_{c2} = J_c \frac{d\omega_c}{dt} \tag{22}$$

Differentiating both sides of formula (22), it can be obtained that:

$$\frac{d_{T_{mf}}}{d_t} - \frac{d_{T_{c2}}}{d_t} = J_c \frac{d_{\omega_c}}{d_t} \tag{23}$$

Discretize formula (23) to obtain:

$$T_{c2}(k) = T_{c2}(k-1) + T_{mf}(k) - T_{mf}(k-1) - J_c \frac{\omega_c(k) - 2\omega_c(k-1) + \omega_c(k-2)}{t_s} \tag{24}$$

The equation at k+1 time:

$$T_{c2}(k+1) = T_{c2}(k) + T_{mf}(k+1) - T_{mf}(k) - J_c \frac{\omega_c(k+1) - 2\omega_c(k) + \omega_c(k-1)}{t_s} \tag{25}$$

Discretize formula (22) to obtain:

$$\omega_c(k) = \omega_c(k-1) + \frac{t_s}{J_C}T_{mf}(k) - \frac{t_s}{J_C}T_c(k) \tag{26}$$

The equation at k+1 time:

$$\omega_c(k+1) = \omega_c(k) + \frac{t_s}{J_c}T_{mf}(k+1) - \frac{t_s}{J_c}T_{c2}(k+1) \tag{27}$$

The discrete state variables are:

$$x(k) = \begin{bmatrix} \omega_c(k) & \omega_c(k-1) & T_{c2}(k) & T_{c2}(k-1) \end{bmatrix}^T \tag{28}$$

The control variables are:

$$u(k) = \begin{bmatrix} T_{mf}(k) & T_{mf}(k-1) \end{bmatrix}^T \tag{29}$$

The state space expression of the system can be obtained as follows, combined with the above equation.
$\begin{bmatrix} \omega_c(k+1) \\ \omega_c(k) \\ T_{c2}(k+1) \\ T_{c2}(k) \end{bmatrix} =$

$$\begin{bmatrix} 0 & 0.5 & -\frac{t_s}{J_c} & 0 \\ 0 & 0 & 0 & -\frac{t_s}{2J_c} \\ -\frac{J_c}{t_s} & \frac{J_c}{t_s} & 0 & 1 \\ 0 & 0 & 0 & 1 \end{bmatrix} \begin{bmatrix} \omega_c(k+1) \\ \omega_c(k) \\ T_{c2}(k+1) \\ T_{c2}(k) \end{bmatrix}.$$

$$+ \begin{bmatrix} 0.5 & 0 & 0 & 0 \\ 0 & 1 & -\frac{t_s}{2J_c} & 0 \\ -\frac{J_c}{t_s} & \frac{J_c}{T_s} & 0 & 0 \\ 0 & 0 & 0 & 0 \end{bmatrix} \begin{bmatrix} \omega_c(k) \\ \omega_c(k\text{-}1) \\ T_{c2}(k) \\ T_{c2}(k\text{-}1) \end{bmatrix} + \begin{bmatrix} \frac{t_s}{J_c} & 0 \\ 0 & \frac{t_s}{J_c} \\ -1 & 1 \\ 0 & 0 \end{bmatrix} \begin{bmatrix} T_{mf}(k+1) \\ T_{mf}(k) \end{bmatrix} \tag{30}$$

Equation(30) can be abbreviated as:

$$x(k+1) = A_1 x(k+1) + A_2 x(k) + B_1 u(k) \tag{31}$$

Through matrix change, equation (31) can be rewritten as:

$$x(k+1) = Ax(k) + Bu(k) \tag{32}$$

$$y(k+1) = Cx(k+1) + Du(k) \tag{33}$$

$$A = (E - A_1)^{-1}A_2, B = (E - A_1)^{-1}B_1 \tag{34}$$

The coefficient matrix in formulas (32) and (33) is:

$$A = \begin{bmatrix} 0 & 0.5 & 0 & 0 \\ -1 & 2 & 0 & 0 \\ 0 & 0 & 0 & 0 \\ 6200 & -6200 & 0.3 & 0 \end{bmatrix} \quad B = \begin{bmatrix} 0.0001 & 0.0003 \\ -0.0004 & 0.0006 \\ 0 & 0 \\ 2.6667 & -2 \end{bmatrix}.$$

$$C = \begin{bmatrix} 1 & 0 & 0 & 0 \end{bmatrix}.$$
$$D = 0.$$

4.3. Torque dynamic coordinated control strategy

According to the flow chart of mode switching designed in this paper, the torque DCCS is an essential component during the mode switching process. Among them, the most important is the DCCS of motor torque and clutch friction torque. During the mode switching process, the friction torque generated by the clutch can cause fluctuations in the total torque of the transmission output shaft. Therefore, the advantages of fast dynamic response and easy control of the motor can be utilized to compensate for the friction torque

of the clutch in real time.

Taking the clutch and motor as a driving system, on the basis that the sum of the clutch friction torque and the motor output torque is equal to the driver's required torque, the output torque of the motor is adjusted dynamically in real time according to the estimated friction torque. Fig. 15 shows a schematic diagram of the DCCS for the motor torque to compensate for the friction torque of the clutch.

5. Simulation results and discussion

Based on the MSCS proposed in Section 4, the MSCS model is established in MATLAB, mainly including the AMESim interface module, mode switching control module based on Stateflow, and control module at each stage of the mode switching process. By setting the S-function interface module in MATLAB/Simulink and the interface block module in AMESim, the signal interaction between the vehicle model built by AMESim and the MSCS model established in MATLAB can be realized to complete the establishment of the co-simulation platform based on AMESim and MATLAB. Taking the switching from Mode SP to Mode DP as an example, the pseudocode corresponding to the control strategy during the mode switching process is shown in Table 5.

5.1. Switch from mode SP to mode DP

Based on the co-simulation platform of AMESim and MATLAB, the MSCS proposed in this paper is simulated and analyzed. The simulation results are shown in Fig. 16.

As shown in Fig. 16 (a) and (b), mode switching starts at 11.06s, the system enters the motor speed regulation stage from the single-motor drive stage, and EM1 starts to output torque and carries out active speed regulation control. According to Fig. 16(b), it can be observed that after 11.41s, C2 generated negative torque. Since the C2 was not fully engaged during this stage, it was unable to transmit the output torque from EM1 (positive torque). Hence, the negative torque generated by C2 was estimated using the KFA. At the same time, during this stage, there was a sudden change in the output torque of EM2, mainly because the output torque of EM2 dynamically changed based on the estimated torque of C2, and the change in output torque of EM2 indirectly proved the effectiveness of clutch estimation torque. As can be seen from Fig. 16 (c), in the motor speed regulation stage, the establishment of oil pressure in the empty stroke stage of C2 is completed synchronously, which is ready for the rapid engagement of C2 after the EM1 speed regulation is completed. As shown in Fig. 16 (a), at 11.41s, the speeds at both ends of the C2 are basically synchronous and the C2 begins to engage. The clutch will generate friction torque during engagement. As seen from Fig. 16 (b), in the clutch sliding friction stage, the EM2 dynamically compensates the friction torque generated by the C2. As seen from Fig. 16 (d) and (e), the sliding friction work generated by C2 is 46.9 J, and the maximum longitudinal jerk during mode switching process is 4.96 m/s^3. Furthermore, as shown in Fig. 16 (e), before 11.41s, the longitudinal jerk is 0, mainly due to the fact that only EM2 drives the vehicle during this stage, and the output torque of EM2 is a constant value. Starting from 11.41s, the longitudinal jerk shows a trend of first slightly decreasing (negative value) and then gradually increasing (positive value). After 11.41s, the mode switching process is in the C2 engagement stage, during which there is a slight sudden change in the longitudinal jerk. The main reason for the slight sudden change in longitudinal jerk is that C2 begins to slip, and the friction torque generated by C2 is transmitted to the output shaft of the gearbox, resulting in a decrease in the total torque transmitted to the vehicle's drive shaft, resulting in negative acceleration; Subsequently, after C2 is fully engaged, with the intervention of EM1 torque, the total torque of the gearbox output shaft and the vehicle drive shaft gradually increases and tends to flatten, and the trend of longitudinal jerk change at this time is related to the cycle conditions.

5.2. Switch from mode DP to mode PD

Based on the co-simulation platform of AMESim and MATLAB, the MSCS from Mode DP to Mode PD is simulated and analyzed. The simulation results are shown in Fig. 17.

As can be seen from Fig. 17 (a), (b) and (c), before 10.61s, EM1 and EM2 jointly drive the vehicle. It can be seen from Fig. 17 (c) at 10.61s that C1 starts to charge oil, indicating that the system starts switching modes. As the oil pressure of C1 increases, C1 enters the sliding stage. As can be seen from Fig. 17 (b), the EM2 dynamically compensates the friction torque generated by the C1 in the sliding stage in real time. At the same time, under the drag of the friction torque of the C1, the engine speed gradually increases. As shown in
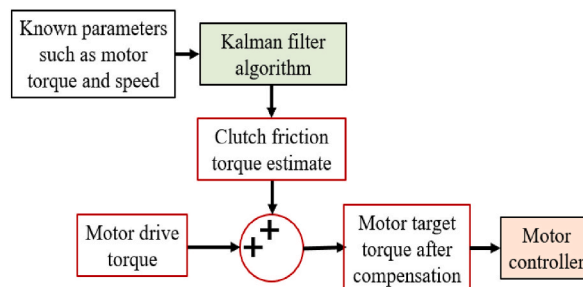
Fig. 15. Schematic diagram of motor torque compensation clutch friction torque.

Table 5
Code for mode switching strategy.

Algorithm 1 : Code for mode switching strategy	
1 :	$C_{st1\_2} \rightarrow$ Control signal of stage1 to stage2
2 :	$C_{st2\_3} \rightarrow$ Control signal of stage2 to stage3
3 :	$C_{st3\_4} \rightarrow$ Control signal of stage3 to stage4
4 :	$W_{EM1\_target} \rightarrow$ Target speed of EM 1
5 :	$W_{EM1\_actual} \rightarrow$ Actual speed of EM 1
6 :	$W_{C2\_active} \rightarrow$ The speed of the active end of C2
7 :	$W_{C2\_driven} \rightarrow$ The speed of the driven end of C2
8 :	$T_{EM1\_control} \rightarrow$ Torque control signal of EM 1
9 :	$P_{C2\_hold} \rightarrow$ Working oil pressure of C2
10 :	$P_{C2\_actual} \rightarrow$ Actual oil pressure of C2
11 :	$P_{C2\_control} \rightarrow$ Control oil pressure of C2
12 :	$C_{st1\_2} \leftarrow 0$
13 :	$C_{st2\_3} \leftarrow 0$
14 :	$C_{st3\_4} \leftarrow 0$
15 :	**while** ($C_{st1\_2} = 1$ & $C_{st2\_3} = 0$ & $C_{st3\_4} = 0$), initialize the EM1 and regulates speed. **do**
16 :	$W_{EM1\_target} \leftarrow W_{C2\_driven}$
17 :	**for** i = 1:N
18 :	if abs(W_{EM1_actual}-W_{EM1_target}) > 100
19 :	Compute the control signal Torque of EM1 $T_{EM1\_control}$
20 :	Update the W_{EM1_actual}
21 :	**else**
22 :	$C_{st2\_3} \leftarrow 1$
23 :	$C_{st1\_2} \leftarrow 0$
24 :	$C_{st3\_4} \leftarrow 0$
25 :	**end if**
26 :	**end for**
27 :	**end while**
28 :	**while** ($C_{st2\_3} = 1$ & $C_{st1\_2} = 0$ & $C_{st3\_4} = 0$), build the oil pressure. do
29 :	**for** k = 1:N
30 :	**if** W_{C2_active} != W_{C2_driven}
31 :	Control the torque of the EM2
32 :	Compute the control signal $P_{C2\_control}$
33 :	Update the W_{C2_active}
34 :	**else**
35 :	$P_{C2\_hold} \leftarrow P_{C2\_actual}$
36 :	$C_{st3\_4} \leftarrow 1$
37 :	$C_{st1\_2} \leftarrow 0$
38 :	$C_{st2\_3} \leftarrow 0$
39 :	**break**
40 :	**end if**
41 :	**end for**
42 :	**end while**
43 :	**while** ($C_{st3\_4} = 1$ & $C_{st1\_2} = 1$ & $C_{st2\_3} = 0$), hold the pressure of C2. **do**
44 :	$P_{C2\_control} \leftarrow P_{C2\_hold}$
45 :	**end while**

Fig. 17 (a), at 10.79s, the engine speed reaches the idle speed (700 r/min). At this moment, the engine is ignited and started. In order to avoid sudden changes in system torque after the engine is started, it can be seen from Fig. 17 (c) that after the engine is ignited, the oil pressure of C1 gradually decreases to ensure that C1 no longer transmits torque, which is also ready for engine speed regulation. As can be seen from Fig. 17 (a) and (c), when the speed difference between the driving and driven ends of C1 decreases, the oil pressure of C1 increases rapidly. When the speed of the engine and the EM1 is equal, it marks the end of the mode switching process. It can be seen from Fig. 17 (d) and (E) that the cumulative sliding friction work generated by the C1 during mode switching is 1683.4 J, and the maximum longitudinal jerk is 5.12 m/s^3.

6. Experimental results and analysis

6.1. Establishment of power level HIL test experimental platform

HIL test is a crucial part of the control strategy "V" cycle development process [48,49]. In order to improve the development efficiency of the control strategy and verify its control effect, this paper builds an HIL platform, as shown in Fig. 18. The platform includes the NI PXI platform, a controller, a human-computer interaction interface on the computer, PSV, a current detection module (CDM), a power supply, and other components. Among these components, a rapid prototyping controller is used as the controller. The vehicle model is processed and calculated in real time through the HIL test system's simulation platform to simulate the vehicle's actual operation. The PSV and the HEV model constitute the controlled object in the HIL test system, which is controlled by the

(a) Rotational speed

(b) Torque

(c) Clutch oil pressure

(d) Clutch sliding work

(e) Longitudinal jerk
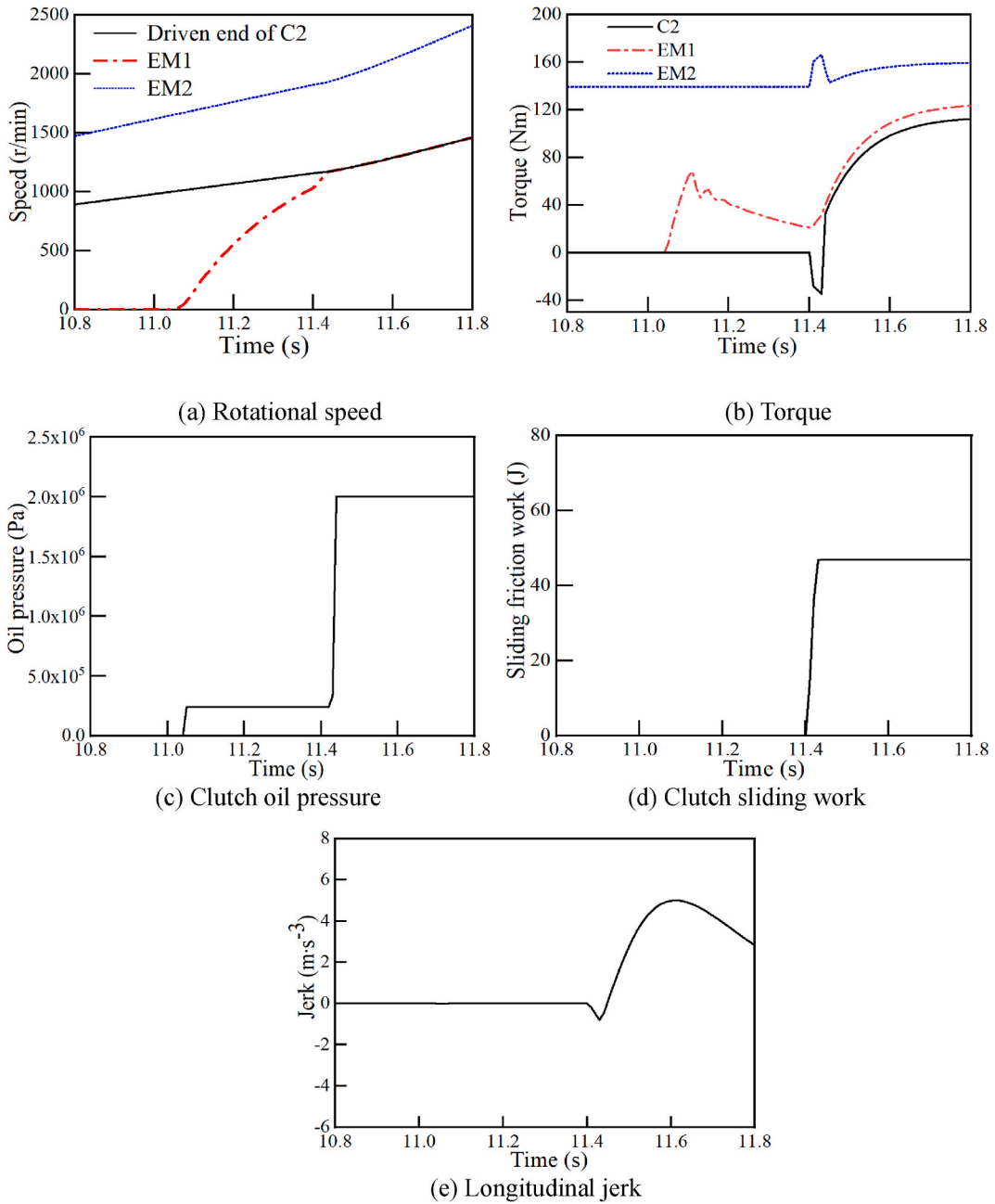
Fig. 16. Simulation results of switching from Mode SP to Mode DP.

controller in the HIL test system. The PSV in the hydraulic system of HPS is added to the HIL test system, and the controller sends the actual power drive signal to control the PSV. The current detection module (CDM) is responsible for processing the signal of the PSV to facilitate the signal interaction between the physical actuator and the virtual simulation model. Through the CDM and simulation platform, data exchange and information transmission can be carried out between the controller and the controlled object, enabling the simulation of the actual working environment of the controller for HIL testing. Additionally, the real-time monitoring and management system serve as the command center of the entire system, allowing adjustment of test parameters and the addition of data recording channels.

6.2. Experimental research on different control strategies

Ref. [50] designed a model predictive controller to control the output torque between various components and the speed of each

(a) Rotational speed

(b) Torque

(c) Clutch oil pressure

(d) Clutch sliding work

(e) Longitudinal jerk
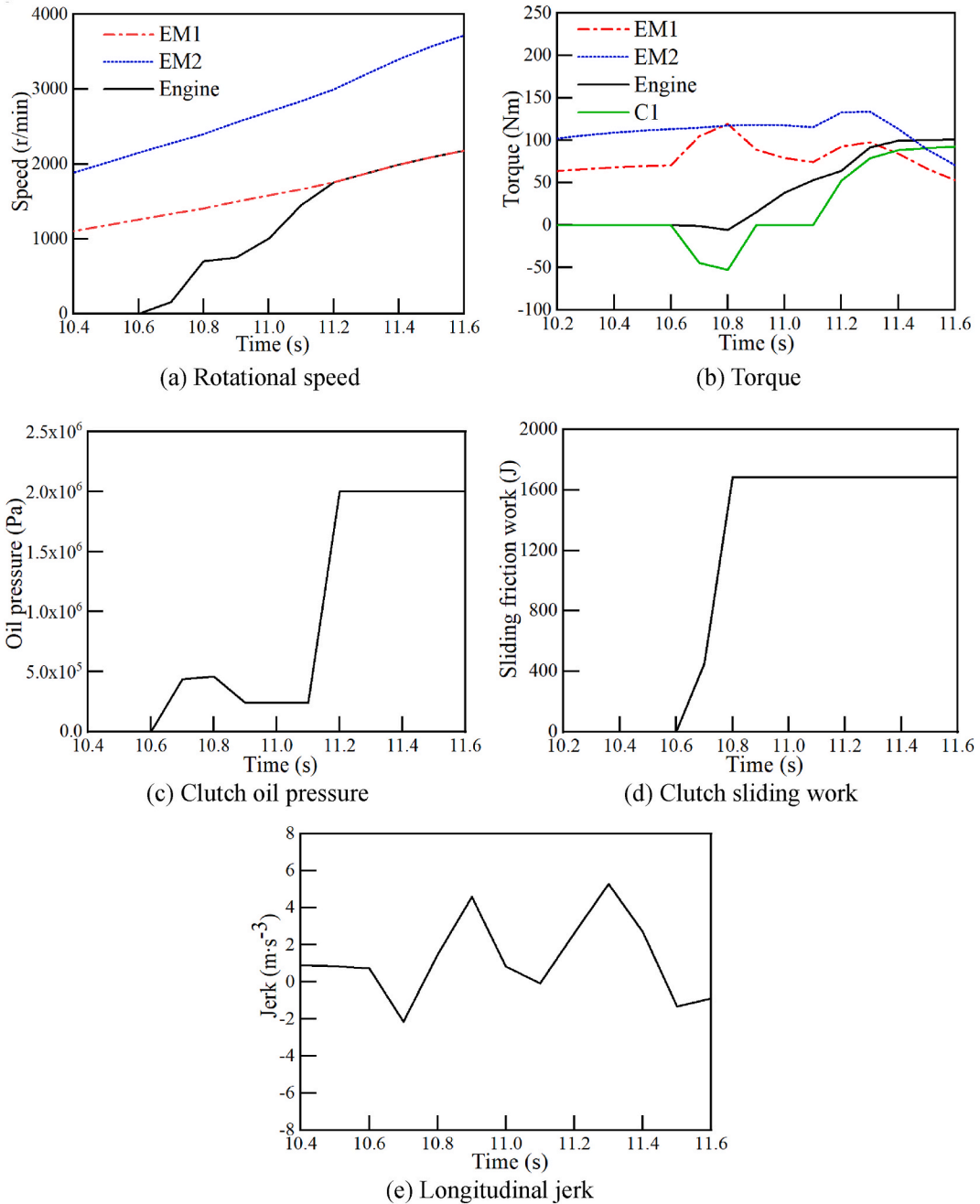
Fig. 17. Simulation results of switching from Mode DP to Mode PD.

shaft to achieve smooth clutch engagement and improve driving comfort. However, the literature didn't introduce the impact of time-varying friction torque during clutch engagement and the DCCS during mode switching. To solve the friction-induced discontinuity during the clutch engagement, previous researchers have investigated adaptive control [51], disturbance observer [23], and fuzzy gain-scheduling control to adapt the nonlinearities of the clutch torque [52]. In addition, the DCCSs that exert the motor torque compensation can also achieve a smooth mode shift [53,54]. This paper establishes an observer model for the friction torque during the clutch engagement process based on the KFA and designs a multi-stage DCCS during the mode switching process. This paper selects the mode switching process from Mode DP to Mode PD as the representative working condition for experimental validation. The control strategy verification experiment of other mode switching is similar. Based on the built power level HIL test platform, the MSCS based on engine idle speed start (Strategy A) and the strategy based on engine target speed start (Strategy B) are compared and analyzed. The main difference between the two MSCSs is the starting mode of the engine (whether the engine is started at idle speed or target speed).
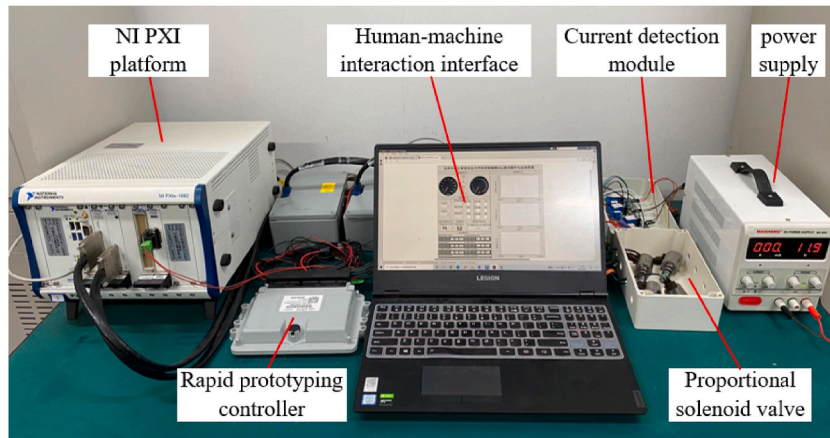
Fig. 18. Power level HIL test bench.

The comparison results of the HIL test of MSCS based on different engine starting speeds are shown in Fig. 19.

It can be seen from Fig. 19 that the start time of mode switching under both MSCSs is 17.52s. As can be seen from Fig. 19 (a) and (b), when the C1 generates friction torque, both MSCSs dynamically compensate for the friction torque of the C1 by using the output torque of the EM1. As can be seen from Fig. 19 (c) and (d), under Strategy B, when the engine speed reaches 700 r/min, the oil pressure of C1 doesn't decrease, and EM1 continues to drag the engine speed up through the friction torque of the C1 until the engine speed is equal to the motor speed at the current time. It can be seen from Fig. 19 (e) that the sliding friction work generated by Strategy A and Strategy B is 2075.7 J and 3611.8 J, respectively, and the sliding friction work generated by Strategy A is reduced by 42.5% compared with Strategy B. The main reason for this difference is that when Strategy B is adopted, the C1 is always in the sliding friction state when the engine speed increases to the speed of EM1, while when Strategy A is adopted, the C1 is adjusted to the disengaged state when the engine speed reaches 700 r/min, so Strategy B produces more sliding friction work. As can be seen from Fig. 19 (f), the maximum values of the longitudinal jerk generated by Strategy A and B are 5.21 m/s^3 and 6.98 m/s^3 respectively, and the maximum value of the longitudinal jerk generated by Strategy A is reduced by 25.4% compared with that generated by Strategy B. There are two main reasons for this. On the one hand, when Strategy A is adopted, the engine speed reaches the idle speed and ignites, and the C1 is quickly separated. Thus it can avoid the torque fluctuation caused by the engine's output torque. On the other hand, when Strategy B is adopted, the engine speed increases directly to the speed of EM1 under the traction of clutch friction torque. After the C1 is engaged, the torque transmitted by the C1 suddenly changes from the friction torque to the engine's output torque. In Ref. [55], a multistage optimal control method has been proposed to facilitate the decision-making process for engine torque and clutch-transmitted torque. The HIL test results illustrate that the jerk intensity remains below 10 m/s^3 throughout the entire mode transition process. Additionally, in Ref. [56], a comprehensive multi-phase engine-start control strategy has been presented. Through simulations and experimental tests, it has been demonstrated that the jerk intensity during the mode switching process is also below 10 m/s^3, thereby meeting the regulatory requirements. These studies serve as important references that validate the effectiveness of our proposed approach in achieving smooth mode transitions and ensuring driving comfort.

7. Conclusions

This paper presents a novel type of dual-motor hybrid power system. Based on the analysis of the system's working mode and modeling principle, the typical mode switching cases are selected, and the control strategy development, simulation and experiment of the mode switching process are conducted. The main findings can be summarized as follows.

1. A model of a novel dual-motor HEV is established based on AMESim software, and a co-simulation platform for researching and developing MSCSs is established based on AMESim and MATLAB.
2. Taking the mode switching process from single motor to dual motor as an example, a torque observer is designed for the friction torque generated in the clutch sliding stage based on KFA and dynamic model.
3. Aiming at the mode switching process of switching from single motor to dual motor, a control strategy of "Motor speed regulation + Clutch friction torque estimation + Motor torque compensation" is proposed. For the mode switching process from dual motors to parallel drive, a control strategy of "Clutch oil pressure control + Clutch friction torque estimation + Motor torque compensation + Engine speed regulation" is proposed. The control strategy designed in this paper is simulated and verified based on the co-simulation platform.
4. Considering the proportional solenoid valve, a power level HIL test platform for studying the control strategy is built in this paper.
5. The mode switching process from dual motors to parallel drive is experimentally tested, and the effects of different engine starting methods on the mode switching process are compared. The results show that compared with the control strategy using the engine
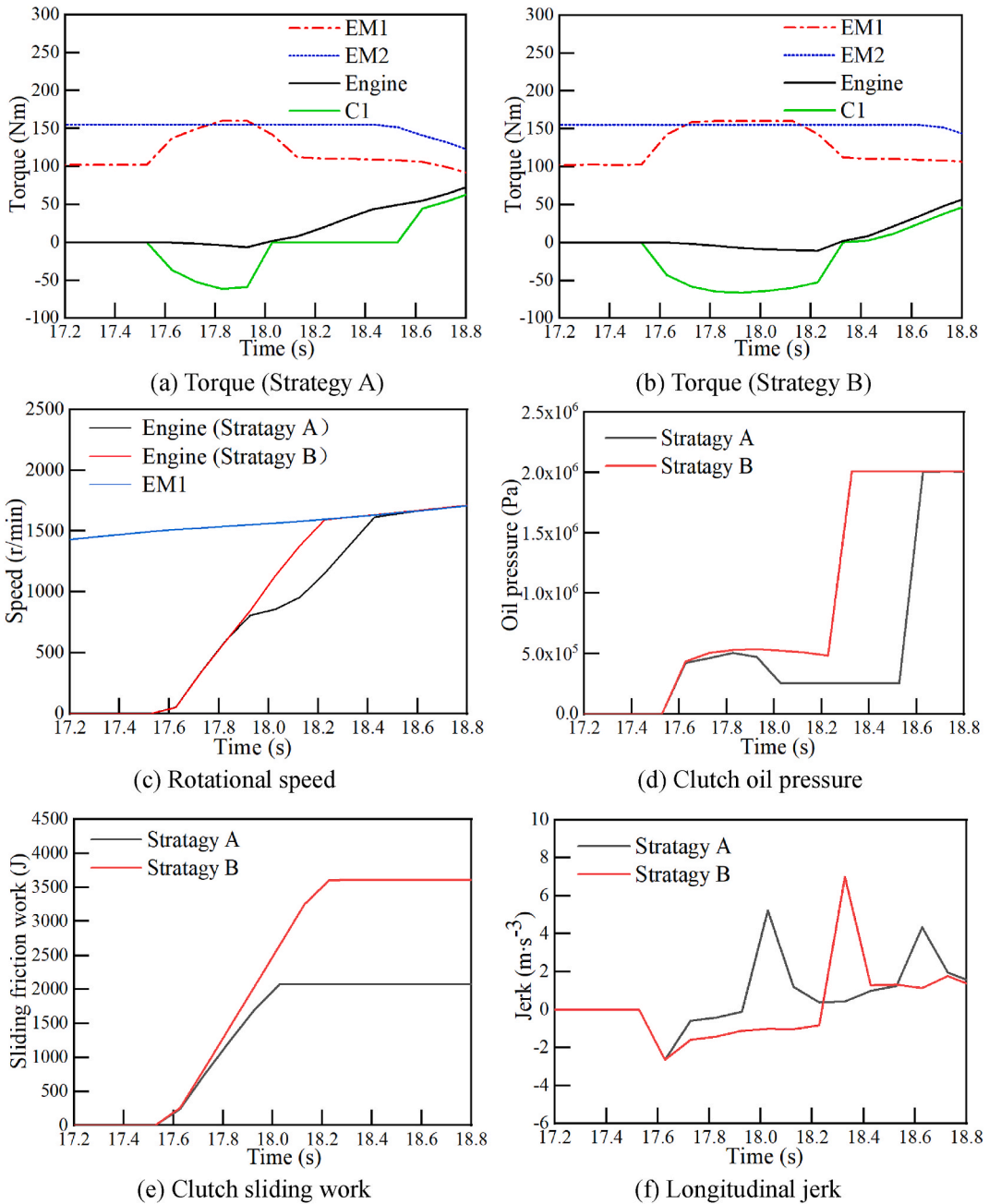
Fig. 19. Test results of different mode switching strategies.

target speed, the control strategy based on engine idle speed proposed in this paper reduces the clutch sliding friction work and the maximum longitudinal jerk of the vehicle by 42.5% and 25.4%, respectively.

In future studies, it would be worthwhile to investigate the effects of torque fluctuations and develop control strategies to mitigate their adverse effects. This research direction would contribute to a comprehensive understanding of the system dynamics during mode transitions and further refine the proposed clutch friction torque observer and dynamic coordinated control strategies. Furthermore, future research can delve deeper into the relationship between clutch friction characteristics and factors such as temperature and oil pressure. This deeper exploration would enhance the existing models and control strategies, providing a more nuanced understanding of the system behavior.

Data availability statement

Data will be made available on request.

CRediT authorship contribution statement

Qicheng Xue: Writing – original draft, Software, Resources, Methodology, Investigation, Conceptualization. **Xin Zhang:** Validation, Supervision, Methodology, Investigation. **Hongwei Chen:** Validation, Software. **Meiling Yue:** Software, Methodology. **Teng Teng:** Writing – review & editing. **Jiangbin Yu:** Writing – review & editing.

Declaration of competing interest

The authors declare that they have no known competing financial interests or personal relationships that could have appeared to influence the work reported in this paper.

Acknowledgment

References

[1] M. Amir, R.G. Deshmukh, H.M. Khalid, et al., Energy storage technologies: an integrated survey of developments, global economical/environmental effects, optimal scheduling model, and sustainable adaption policies, J. Energy Storage 72 (2023) 108694.

[2] X. Dong, B. Zhang, B. Wang, et al., Urban households' purchase intentions for pure electric vehicles under subsidy contexts in China: do cost factors matter, Transport. Res. Pol. Pract. 135 (2020) 183–197.

[3] J.E. Jony, P.B. Társis, F.S. Samuel, et al., Electric hydraulic hybrid vehicle powertrain design and optimization-based power distribution control to extend driving range and battery life cycle, Energy Convers. Manag. 252 (2022) 115094.

[4] M.C. Annamalai, N.A. Prabha, A comprehensive review on isolated and non-isolated converter configuration and fast charging technology: for battery and plug in hybrid electric vehicle, Heliyon 9 (8) (2023) 18808.

[5] M.A. Hafiz, Thermal management systems for batteries in electric vehicles: a recent review, Energy Rep. 9 (2023) 5545–5564.

[6] M.A. Ghadikolaei, P.K. Wong, C.S. Cheung, et al., Why is the world not yet ready to use alternative fuel vehicles, Heliyon 7 (7) (2021) 07527.

[7] R. Chen, C. Yang, L. Han, et al., Power reserve predictive control strategy for hybrid electric vehicle using recognition-based long short-term memory network, J. Power Sources 520 (2022) 230865.

[8] S.M. Adem, M.A. Samson, O.S. Ayodeji, et al., Review of optimal sizing and power management strategies for fuel cell/battery/super capacitor hybrid electric vehicles, Energy Rep. 9 (2023) 2213–2228.

[9] Y. Yang, Y. Xu, H. Zhang, et al., Research on the energy management strategy of extended range electric vehicles based on a hybrid energy storage system, Energy Rep. 8 (2022) 6602–6623.

[10] P. Dong, S. Wu, W. Guo, et al., Coordinated clutch slip control for the engine start of vehicles with P2-hybrid automatic transmissions, Mech. Mach. Theor. 153 (3) (2020) 103899.

[11] B.V. Padmarajan, A. Mcgordon, P.A. Jennings, Blended rule-based energy management for PHEV: system structure and strategy, IEEE Trans. Veh. Technol. 65 (10) (2016) 8757–8762.

[12] K.V. Singh, H.O. Bansal, D. Singh, Fuzzy logic and Elman neural network tuned energy management strategies for a power-split HEVs, Energy 225 (2021) 120152.

[13] W. Sun, Y. Zou, X. Zhang, et al., High robustness energy management strategy of hybrid electric vehicle based on improved soft actor-critic deep reinforcement learning, Energy 258 (2022) 124806.

[14] J. Li, Y. Liu, Y. Zhang, et al., Data-driven based eco-driving control for plug-in hybrid electric vehicles, J. Power Sources 498 (6) (2021) 229916.

[15] Y. Wang, K. Li, X. Zeng, et al., Investigation of novel intelligent energy management strategies for connected HEB considering global planning of fixed-route information, Energy 263 (2023) 125744.

[16] Y. Lin, D. Qin, Y. Liu, et al., Control strategy for all the mode-switches of hybrid electric vehicle, Adv. Mech. Eng. 8 (11) (2016) 1–17.

[17] K. Huang, C. Xiang, Y. Ma, et al., Mode shift control for a hybrid heavy-duty vehicle with power-split transmission, Energies 10 (2) (2017) 1–18.

[18] Y. Liu, D. Chen, Z. Lei, et al., Modeling and control of engine starting for a full hybrid electric vehicle based on system dynamic characteristics, Int. J. Automot. Technol. 18 (5) (2017) 911–922.

[19] R. Chen, C. Yang, Y. Ma, et al., Online learning predictive power coordinated control strategy for off-road hybrid electric vehicles considering the dynamic response of engine generator set, Appl. Energy 323 (2022) 119592.

[20] L. Chen, G. Xi, J. Sun, Torque coordination control during mode transition for a series–parallel hybrid electric vehicle, IEEE Trans. Veh. Technol. 61 (7) (2012) 2936–2949.

[21] J. Sun, G. Xing, X. Liu, et al., A novel torque coordination control strategy of a single-shaft parallel hybrid electric vehicle based on model predictive control, Math. Probl Eng. 2015 (1) (2015) 1–12.

[22] X. Zeng, N. Yang, J. Wang, et al., Predictive-model-based dynamic coordination control strategy for power-split hybrid electric bus, Mech. Syst. Signal Process. 60 (7) (2015) 785–798.

[23] H. Kim, J. Kim, H. Lee, Mode transition control using disturbance compensation for a parallel hybrid electric vehicle, Proc. Inst. Mech. Eng. - Part D J. Automob. Eng. 225 (2) (2011) 150–166.

[24] C. Yang, X. Jiao, L. Li, et al., A robust H∞ control-based hierarchical mode transition control system for plug-in hybrid electric vehicle, Mech. Syst. Signal Process. 99 (3) (2018) 26–44.

[25] R. He, X. Tian, Y. Ni, et al., Mode transition coordination control for parallel hybrid electric vehicle based on switched system, Adv. Mech. Eng. 9 (8) (2017) 1–12.

[26] Y. Qi, C. Xiang, W. Wang, et al., Model predictive coordinated control for dual-mode power-split hybrid electric vehicle, Int. J. Automot. Technol. 19 (2) (2018) 345–358.

[27] F. Zhu, L. Chen, C. Yin, et al., Dynamic modelling and systematic control during the mode transition for a multi-mode hybrid electric vehicle, Proc. Inst. Mech. Eng. - Part D J. Automob. Eng. 227 (7) (2013) 1007–1023.

[28] H.M. Khalid, F. Flitti, S.M. Muyeen, et al., Parameter estimation of vehicle batteries in V2G systems: an exogenous function-based approach, IEEE Trans. Ind. Electron. 69 (9) (2022) 9535–9546.

[29] H.M. Khalid, C.H. Peng, Bi-directional charging in V2G systems: an In-Cell variation analysis of vehicle batteries, IEEE Syst. J. 14 (3) (2020) 3665–3675.

[30] Z. Rafique, H.M. Khalid, S.M. Muyeen, Communication systems in distributed generation: a bibliographical review and frameworks, IEEE Access 8 (2020) 207226–207239.

[31] T. Jin, P. Li, G. Zhu, Optimal Decoupled Control for Dry Clutch engagement[C], IEEE American Control Conference, Washington, DC, USA, 2013.

[32] M. Pisaturo, M. Cirrincione, A. Senatore, Multiple constrained MPC design for automotive dry clutch engagement, IEEE ASME Trans. Mechatron. 20 (1) (2014) 469–480.

[33] C.J. Chiang, Y.C. Chen, C.Y. Lin, Fuzzy sliding mode control for smooth mode changes of a parallel hybrid electric vehicle[C]//, in: IEEE International Conference on Control & Automation (ICCA), Taichung, Taiwan, 2014.

[34] B. Gao, H. Chen, Y. Hu, et al., Nonlinear feedforward-feedback control of clutch-to-clutch shift technique, Veh. Syst. Dyn. 49 (12) (2011) 1895–1911.

[35] Y. Chao, X. Jiao, L. Liang, et al., A robust H∞ control-based hierarchical mode transition control system for plug-in hybrid electric vehicle, Mech. Syst. Signal Process. 99 (15) (2018) 326–344.

[36] J. Park, S. Choi, J. Oh, et al., Adaptive torque tracking control during slip engagement of a dry clutch in vehicle powertrain, Mech. Mach. Theor. 134 (2019) 249–266.

[37] Z. Zhao, D. Lei, J. Chen, et al., Optimal control of mode transition for four-wheel-drive hybrid electric vehicle with dry dual-clutch transmission, Mech. Syst. Signal Process. 105 (2018) 68–89.

[38] A.M. Gavgani, A. Sorniotti, J. Doherty, et al., Optimal gearshift control for a novel hybrid electric drivetrain, Mech. Mach. Theor. 105 (2016) 352–368.

[39] F. Meng, H. Chen, T. Zhang, et al., Clutch fill control of an automatic transmission for heavy-duty vehicle applications, Mech. Syst. Signal Process. 64–65 (2015) 16–28.

[40] S. Li, C. Wu, Z. Sun, Design and implementation of clutch control for automotive transmissions using Terminal-Sliding-Mode control and uncertainty observer, IEEE Trans. Veh. Technol. 65 (4) (2016) 1890–1898.

[41] S. Wang, Y. Liu, Z. Wang, et al., Adaptive fuzzy iterative control strategy for the wet-clutch filling of automatic transmission, Mech. Syst. Signal Process. 130 (2019) 164–182.

[42] F. Meng, G. Tao, H. Chen, Smooth shift control of an automatic transmission for heavy-duty vehicles, Neurocomputing 159 (2) (2015) 197–206.

[43] G. Tao, M. Wu, F. Meng, Online performance evaluation of a heavy-duty automatic transmission launching process, Mechatronics 38 (2016) 143–150.

[44] Z. Wei, J. Soheil, S. Zhang, et al., Hybrid wiener model: an on-board approach using post-flight data for gas turbine aero-engines modelling, Appl. Therm. Eng. 184 (2021) 116350.

[45] M. Yue, A.M. Zeina, J. Samir, et al., An online prognostics-based health management strategy for fuel cell hybrid electric vehicles, Int. J. Hydrogen Energy 46 (24) (2021) 13206–13218.

[46] F. Zhang, Y. Hu, J. Xi, et al., The coordinate control strategy of torque recovery for the parallel hybrid electric vehicle, Asian J. Control 18 (1) (2016) 40–54.

[47] D. Wei, H. He, J. Cao, Hybrid electric vehicle electric motors for optimum energy efficiency: a computationally efficient design, Energy 203 (2020) 117779.

[48] X. Lin, J. Wu, Y. Wei, An ensemble learning velocity prediction-based energy management strategy for a plug-in hybrid electric vehicle considering driving pattern adaptive reference SOC, Energy 234 (2021) 121308.

[49] S. Ruan, Y. Ma, N. Yang, et al., Real-time energy-saving control for HEVs in car-following scenario with a double explicit MPC approach, Energy 247 (2022) 123265.

[50] V.T. Minh, F. Hashim, M. Awang, Development of a real-time clutch transition strategy for a parallel hybrid electric vehicle, Proc. Inst. Mech. Eng. 226 (2) (2012) 188–203.

[51] G. Shi, P. Dong, H. Sun, et al., Adaptive control of the shifting process in automatic transmissions, Int. J. Automot. Technol. 18 (1) (2017) 179–194.

[52] F. Zhu, L. Chen, C. Yin, et al., Dynamic modelling and systematic control during the mode transition for a multi-mode hybrid electric vehicle, Proc. Inst. Mech. Eng. - Part D J. Automob. Eng. 227 (7) (2013) 1007–1023.

[53] C. Wang, Z. Zhao, T. Zhang, et al., Mode transition coordinated control for a compound power-split hybrid car, Mech. Syst. Signal Process. 87 (PT.A) (2017) 192–205.

[54] K. Huang, C. Xiang, M. Yue, et al., Mode shift control for a hybrid heavy-duty vehicle with power-split transmission, Energies 10 (2) (2017) 177.

[55] Z. Zhao, D. Lei, J. Chen, Optimal control of mode transition for four-wheel-drive hybrid electric vehicle with dry dual-clutch transmission, Mech. Syst. Signal Process. 105 (2018) 68–89.

[56] C. Zhao, B. Zu, Y. Xu, et al., Design and analysis of an engine-start control strategy for a single-shaft parallel hybrid electric vehicle, Energy 202 (2020) 117621.